Rare Metal Materials and Engineering
Volume 45, Issue 6, June 2016
Online English edition of the Chinese language journal

Available online at www.sciencedirect.com
ScienceDirect

Cite this article as: Rare Metal Materials and Engineering, 2016, 45(6): 1374-1380.

ARTICLE

In Situ Characterization on Thermal Transitions of VO_2(B): Toward VO_2(R) and V_2O_3

Zhang Shaohong, Fu Juan, Su Qiucheng, Wu Liangpeng, Li Xinjun

Guangzhou Institute of Energy Conversion, Chinese Academy of Sciences, Guangzhou 510640, China

Abstract: VO_2(B) was synthesized via a facile hydrothermal process using V_2O_5 and oxalic acid. The crystal structure and the phase transition of VO_2(B) during elevated temperatures in N_2 were investigated by in situ X-ray diffraction (XRD). Meanwhile, the morphologies and the crystal structures of the samples obtained by annealing at different temperatures were characterized by Field emission scanning electron microscopy (FE-SEM), XRD and Raman spectroscopy, respectively. The results show that the as-synthesized nano platelet-like monoclinic VO_2(B) irreversibly transforms into submicron and micron subsphaeroidal tetragonal VO_2(R) between 430 and 700 °C. The as-obtained VO_2(R) starts to decompose and form Magnéli phases V_nO_{2n-1} ($3 \le n \le 9$) series compounds at ~1000 °C, and totally transfers into a corundum V_2O_3 sintered block at ca. 1200 °C.

Key words: hydrothermal; vanadium oxides; in situ XRD; thermal transformation

Vanadium (V) is the fifth most abundant transition metal in the earth. Unlike its neighboring transitional metals such as Ti, Cr and Mn, V exists with numerous possible valencies and, consequently, has many different oxides [1]. Among these compounds, V_2O_3, VO_2, and V_2O_5 have been widely studied as optical, electrical, electrochemical, thermochromic and thermal switching materials [2]. VO_2, in particular, has attracted tremendous attention as they exhibit different structures with distinctive optical and electrical properties [3-5].

So far, more than ten crystalline phases of VO_2 have been reported [6], including tetragonal VO_2(R) (P42/mnm) [7], monoclinic VO_2(M) (P21/c) [8,9], tetragonal VO_2(A) (P42/nmc) [10], monoclinic VO_2(B) (C2/m) [11] and VO_2(C) [12]. Out of these phases, VO_2(M) is considered to be the most stable and attracts much interest because it undergoes a reversible transition to VO_2(R) at approximately 68 °C [13,14], its conductivity and optical transmittance change abruptly through the phase transition [15], and it can be used in thermochromic coatings [16], temperature sensing devices [17], optical switching devices [4,18,19] and Mott field-effect transistors [20]. Except VO_2(M/R), VO_2(B) with metastable monoclinic structure is of great interest, owing to its high energy capacity along with moderate work potential, and its promising applications in the field of energy technologies [21-24]. Besides, VO_2(B) is usually used as the precursor of VO_2(M/R) [25-27]. The transformation of VO_2(B) →VO_2(R) was first reported at 400~450 °C by Théobald et al. [11]. Later, it was studied by thermogravimetry (TG), differential scanning calorimetry (DSC), Fourier transform infrared spectroscopy (FT-IR), and in situ electron microscopy methods [23, 27-29]. And it was shown that it was not a first-order transformation occurring at a fixed temperature. It varied from 320 to 500 °C. But, recently, Li and his coworkers have found that the transformation did not complete even when the temperature was kept at 500 °C for 4 h, and they called for a further investigation to confirm the process [30]. Meanwhile, they also pointed out that the researches on the phase transition of VO_2 had significant senses for preparing excellent materials [31]. Owing to the

Received date: May 24, 2015
Foundation item: National Natural Science Foundation of China (51172233); the Development of Instrument & Equipment Function and Technical Innovation Project of CAS and the Analytical & Testing Fund of Guangzhou Area, China (201212)
Corresponding author: Su Qiucheng, Ph. D., Professor, Key Laboratory of Renewable Energy, Guangzhou Institute of Energy Conversion, Chinese Academy of Sciences, Guangzhou 510640, P. R. China, Tel: 0086-20-37246206, E-mail: suqc@ms.giec.ac.cn

complex mechanism and its great importance to VO_2 materials preparation and application, many efforts have been made to investigate the transformation of VO_2(B). However, there is still limited amount of literatures revealing the thermal transition of the VO_2(B) in detail by far.

Thus, the aim of the present work is to present a more detailed characterization of VO_2(B) thermal transition. An in situ XRD method was employed to investigate the as-synthesized VO_2(B) transition during the process of elevated temperature up to 1200 °C in N_2. Our work provided new insights into the VO_2(B) → VO_2(R) transition. We also observed the structure, morphology and Raman spectrum evolution of the sample from monoclinic VO_2(B) to tetragonal VO_2(R)/monoclinic VO_2(M), and to rhombohedral V_2O_3.

1 Experiment

All the chemical reagents used in the present experiment were analytical grade. In a typical procedure, 0.9 g vanadium pentaoxide (V_2O_5; Tianjin Fuchen chemical reagents factory) and 1.26 g oxalic acid dihydrate ($H_2C_2O_4 \cdot 2H_2O$; Jiangsu Qiangsheng Fuctional Chemical Ltd.) were dispersed in 50 mL deionized water. After stirring for 30 min at 60 °C, the resulting yellow suspension was transferred to 90 mL Teflon-lined stainless steel autoclave and hydrothermally treated for 24 h at 180 °C. After cooling down to room temperature, the resulting powder was washed with deionized water and ethanol, and dried at 60 °C for 12 h. The final obtained blue powder was marked as S-180. The samples annealed at 450, 600, 750 and 1200 °C were named as S-450, S-600, S-750 and S-1200, respectively.

Phase identification was carried out via XRD analysis on a PANalytical diffractometer (X'Pert Pro MPD) using Cu $K\alpha_{1,2}$ radiation (λ = 0.1 540 598, 0.1 544 426 nm) at 40 kV accelerating voltage and 40 mA. Experiments were performed both at elevated temperatures for in situ XRD study and at ambient temperature for further confirmation of the results. In situ XRD was carried out with an Anton Paar HTK 1200N high-temperature chamber. The chamber was used to heat up the sample with a control accuracy of ± 2 °C in a flow controlled N_2 environment. The sample was heated to 1200 °C at a fixed heating rate of 10 °C·min^{-1}. The diffraction data were obtained in the 2θ range between 10 and 80° with a 0.0167° step size and 10 s dwell time. The identification of the compounds was made by comparing the experimental XRD patterns to standards compiled by the Joint Committee on Powder Diffraction and Standards (JCPDS). The alignment was done at ambient temperature with a standard of silicon crystalline powder.

Morphologies and microstructure of the samples were observed by FE-SEM (HITACHI S-4800). Samples were directly deposited on an aluminum stub using double-sided adhesive carbon tape. Images were observed and captured under 2.0 or 3.0 kV accelerating voltage and 10.0 μA emission current.

Raman spectra of samples were recorded on LabRAM HR 800 high resolution spectrometer (Horiba Jobin Yvon). The spectral resolution was about 1 cm^{-1}. Samples were excited by a Nd:YAG laser (λ = 532.16 nm, 50 mW maximum output power) fed through an integral confocal microscope, focused onto the sample with an Olympus MPLN50x micro-objective. The light scattered from the sample was collected with the same objective in backscattering (180°) geometry. To minimize laser irradiate injuring of the sample, the incident beam was attenuated before it entered the microscope. Calibration was performed during measurements with a silicon semiconductor mode at 520.7 cm^{-1}.

2 Results and Discussion

2.1 In situ XRD analysis

The evolution of the diffraction patterns of the as-synthesized sample during elevated temperature in situ XRD is presented in Fig.1, accompanied with JCPDS No. 081-2392, No. 076-0678, No. 009-8711, No. 071-0041 and No. 071-0343. The sample was heated from 30 °C to 100 °C, followed by heating at 100 °C increments to 400 °C, at 10 °C increments to 1000 °C and at 50 °C increments to 1200 °C. At 30 °C, the observed diffraction pattern can be indexed to the monoclinic VO_2(B) (JCPDS No. 081-2392), and this remains predominant phase up to 420 °C (see Fig.1 curve 1~ 8). At 430 °C, a small shoulder appears at 27.5° (2θ), and as the temperature increases, more other peaks are observed. These peaks become prominent when the heating temperature increases to 700 °C. All the peaks can be indexed to tetragonal VO_2(R) (JCPDS No. 076-0678). No other peaks are observed (see Fig.1 curve 9~ 16 and 21). But, there is a slight shift (–0.2°~–0.7°) in the elevated temperature experimental diffraction peak positions, compared with calculated tetragonal VO_2(R) (110), (101), (200), (111), (210), (211), (220), (310), (002), (301), (112) and (311) reflections. The slight shift can be attributed to the thermal expansion [32]. From 430 °C to 690 °C, the emergence of VO_2(R) couples with a decrease of the VO_2(B) phase. At 700 °C, VO_2(B) phase completely disappears and VO_2(R) becomes the sole phase. Thus, we consider that the as-synthesized VO_2(B) shows moderate thermal stability and remains unchanged from room temperature to 420 °C in N_2 atmosphere. The VO_2(B)→ VO_2(R) transition undergoes a sluggish process, starting at around 430 °C, and finishing at ~700 °C. Both the onset and offset temperature are lower than that in previous reports [33]. It may be attributed to the lower heating rate and the influence of VO_2(B) synthesis techniques and its initial morphologies [30].

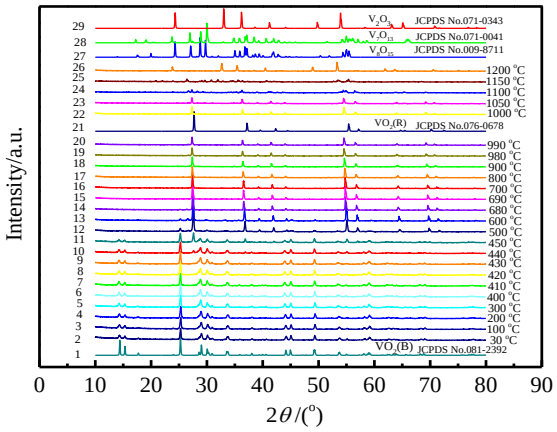

Fig.1 In situ XRD patterns of VO_2(B) collected at elevated temperature from 30~1200 °C, at 10 °C min^{-1} heating rate, under N_2 flow atmosphere and VO_2(B), VO_2(R), V_8O_{15}, V_7O_{13}, V_2O_3 JCPDS simulation patterns. Note the emergence of the VO_2(R) at 430 °C, which becomes the sole phase at 700 °C; the emergence of Magnéli phases at 1000 °C, V_2O_3 becomes the sole phase at 1200 °C

From 700 to 990 °C, VO_2(R) phase remains predominant (see Fig.1 curve 16~20). Diffraction peaks other than VO_2(R) phase emerge at 1000 °C, and the peaks become predominate with the increase of the temperature, and they may be indexed to Magnéli phases V_nO_{2n-1} ($3\leq n\leq 9$) series compounds, such as anorthic V_8O_{15} (JCPDS No. 009-8711), anorthic V_7O_{13} (JCPDS No. 071-0041) and rhombohedral V_2O_3 (JCPDS No. 071-0343). At 1150 °C, VO_2(R) phase disappears completely. At 1200 °C, all diffraction peaks of the sample are indexed to the rhombohedral phase of V_2O_3 (JCPDS No. 071-0343) (see Fig.1 curve 22~ 29). From the experiments, we consider that the as-obtained VO_2(R) is not as stable as that reported in range of 68 to 1540 °C [27]. It may be attributed to the influence of the microstructure and the morphology of its precursor. In the present work, the rutile VO_2(R) is originated from nanostructure VO_2(B), and is prone to decompose to produce series Magnéli phases compounds. The decomposition of VO_2(R) emerges at 1000 °C.

Thus, from the above in situ XRD experiments analysis, we consider that the as-synthesized sample is monoclinic phase VO_2(B). During the process of elevated temperature from 30 to 1200 °C in N_2, there is no obvious change at 30 ~ 420 °C in monoclinic phase VO_2(B), and rutile structure VO_2(R) coexists with the monoclinic VO_2(B) between 430 and 690 °C. The emergence of VO_2(R) couples with a decrease of VO_2(B) phase with the increase of the temperature. From 700 °C to 990 °C, VO_2(R) becomes the sole phase. At 1000 °C, VO_2(R) starts to decompose to produce series Magnéli phases compounds. At 1150 °C, VO_2(R) phase disappears completely. Finally, the rhombohedral phase of V_2O_3 is obtained at 1200 °C. The crystal phase and the structure evolution can be presented in Table 1. Monoclinic VO_2(B) exhibits a typical layer structure, layers of edge-sharing along the *ab* plane [VO_6] octahedra are connected by corners to form a three-dimensional crystal structure. V atoms deviate from the center of the oxygen octahedra. It leads to two types of deformed octahedra. Tetragonal VO_2(R) has a more symmetric structure. V atoms are at the center of the regular oxygen octahedra. With respect to vanadium site it is based on a body-centered tetragonal lattice. [VO_6] octahedra at the corners and the center of a unit cell are rotated by 90 ° around the *c*-axis. Adjacent [VO_6] octahedral shares edges to form chains along the *c*-axis. Corner and center chains are connected via corners. Rhombohedral V_2O_3 is based on a trigonal lattice with space group R-3c. The oxygen atom is arranged qualitatively to be equivalent to the network in VO_2. V atoms fill only two thirds of oxygen octahedra. Two filled followed by one empty face-sharing octahedra form noncontinuous chains along *c*-axis. The Magnéli phases can be considered as $V_nO_{2n-1}=V_2O_3+(n-2)\ VO_2$ ($3\leq n\leq 9$) [34]. As is obvious from the stoichiometric relation, their crystal structures comprise dioxide and sesquioxide-like regions, respectively. Clearly, VO_2(B) and VO_2(R) have totally different arrangements of [VO_6] octahedra crystal structure. The transition from VO_2(B) to VO_2(R) leads a dramatic rearrangement and reshuffling within the structure. It likely is so-called reconstructive solid state phase transformation. It can explain why the VO_2(B)→VO_2(R) transition

Table 1 Summary of the crystal structure evolution at elevated temperatures

Temperature/°C	Phase indexed	Crystal structure
30~420	Monoclinic VO_2(B)	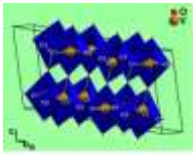
430~690	Monoclinic VO_2(B) + tetragonal VO_2(R)	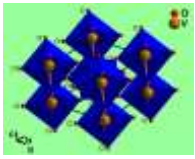
700~990	Tetragonal VO_2(R)	
1000~1140	Tetragonal VO_2(R) + Magnéli phases V_nO_{2n-1} ($3\leq n\leq 9$)	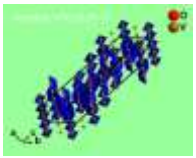
1150~1190	Magnéli phases V_nO_{2n-1} ($3\leq n\leq 9$) + rhombohedral V_2O_3	
1200	Rhombohedral V_2O_3	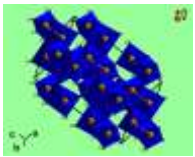

undergoes a sluggish process and covers a wide temperature range.

2.2 XRD analysis

The as-synthesized VO_2(B) (S-180) and samples annealed at different temperatures were also characterized by XRD at ambient temperature. In Fig.2, all these XRD results are compared with the JCPDS standards. The experimental pattern of samples S-180, S-750 and S-1200 can be indexed to the monoclinic phase of VO_2(B) (JCPDS No. 081-2392), monoclinic phase of VO_2(M) (JCPDS No. 082-0661) and rhombohedral phase of V_2O_3 (JCPDS No. 071-0343), respectively. According to previous works[13,14], VO_2(M) undergoes a reversible phase transition to VO_2(R) at approximately 68 °C, so the result can further confirm the formation of VO_2(R). Comparing curves 4 and 5 with curves 1 and 3 in Fig.2, both the spectra of S-450 and S-600 have the VO_2(B) and VO_2(M) characteristic diffraction peaks. The result reveals that sample S-450 and S-600 are mixtures of VO_2(B) and VO_2(M). It is consistent with the above in situ XRD analysis.

In summary, the results agree with those obtained during the above in situ XRD analysis. The difference is: at high temperature there is a slight shift in the diffraction peak positions, owing to thermal expansion [32]; nevertheless, at room temperature all peaks are highly coincided with the standard patterns. No peaks of any other phases or impurities are detected in these spectra, revealing that the as-prepared products S-180, S-750 and S-1200 are mainly composed of VO_2(B), VO_2(M) and V_2O_3, respectively. Thereby, it can be confirmed that VO_2(B), VO_2(R/M) and V_2O_3 are formation.

2.3 Morphology and microstructure analysis

All the sizes and morphologies of the samples were examined by FE-SEM. Fig.3a reveals the as-synthesized VO_2(B) is composed of polydisperse nano platelets. The particle size is 50~250 nm in width, 15~35 nm in thickness and less than 100 nm to more than 1 μm in length. This morphology is attributed to its layer crystal structure [34,35]. Fig.3b shows the surface and the edge of platelet-like nanostructure get round in sample S-450, but the platelet-like morphology has no prominent change. Fig.3c clearly indicates that most of the nanostructures change from platelet-like morphology to subsphaeroidal morphology in sample S-600, accompanying with a crystal growth. The diameters increase to more than 1 μm alongside smaller nanoparticles. Fig.3d reveals that all of the nanostructure

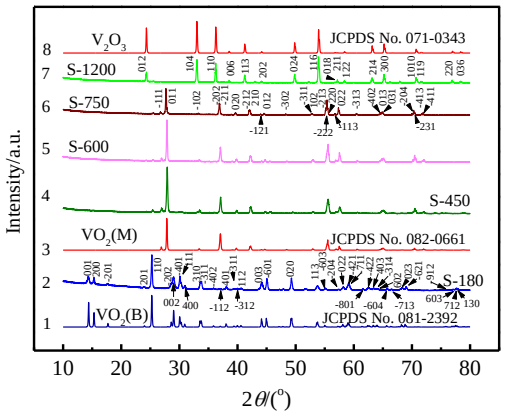

Fig.2 XRD patterns of annealed samples (1: JCPDS No. 081-2392, 2: S-180, 3: JCPDS No. 082-0661, 4: S-450, 5: S-600, 6: S-750, 7: S-1200, 8: JCPDS No. 071-0343)

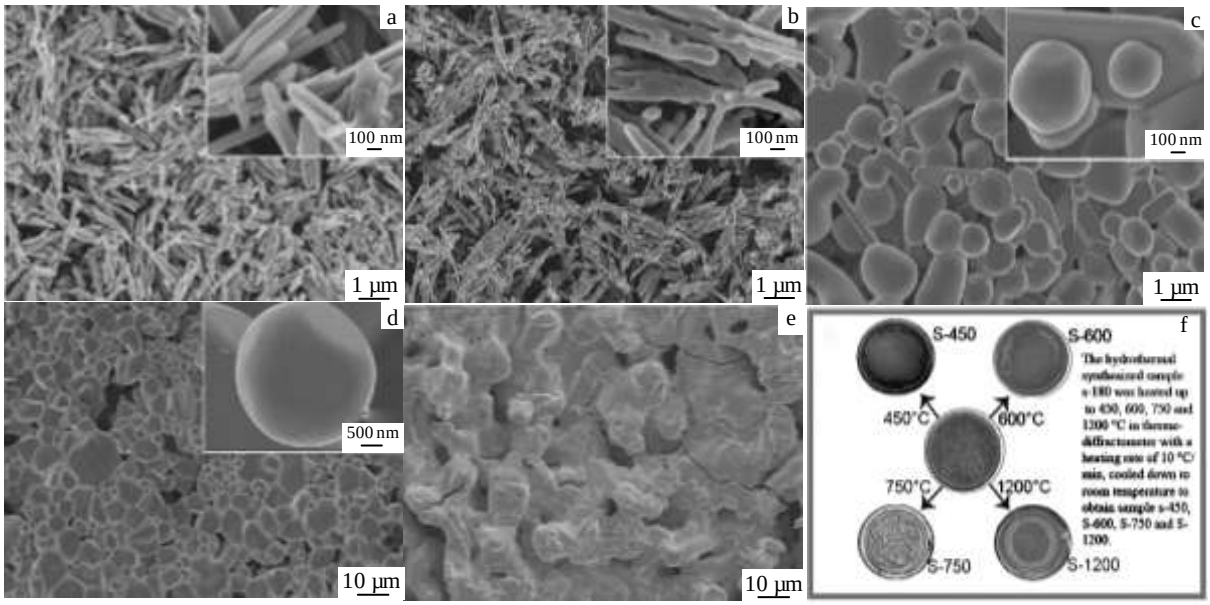

Fig.3 SEM micrograph of VO_2(B) as-synthesized and annealed at different temperatures: (a) S-180, (b) S-450, (c) S-600, (d) S-750, and (e) S-1200, (f) photo of samples in corundum crucible cooled down in situ

changes into submicron and micron subsphaeroidal morphology in sample S-750, and the particle size keeps polydisperse with ~10 μm alongside smaller nanoparticles. Fig.3e indicates that the sample S-1200 becomes one sintered compact. Fig.3f demonstrates the macro morphology evolution of the sample annealed at different temperatures under the N_2 flow atmosphere. At room temperature, the as-synthesized powder is pressed in the crucible (see Fig.3f S-180). At 450 °C, the gap between the powder and edge of the crucible is observed (see Fig.3f S-450). Up to 600 °C, the gap broadens (see Fig.3f S-600). And to 750 °C, cracks in the sample appear (see Fig.3f S-750). When the temperature is up to 1200 °C, the sample is sintered to one block with pores and flaws (see Fig.3f S-1200). These can be attributed to densification, grain growth and powder agglomeration during thermal transformation and sintering. The heating has a pronounced effect on the morphology. And there is a decrease in specific volume during transformation because the density changes from 4.00 g·cm^{-3} [VO_2(B)] to 4.66 g·cm^{-3} [VO_2(R/M)] and 4.92 g·cm^{-3}(V_2O_3). Large crystallites of VO_2(R/M) is obtained by heating nanostructure VO_2(B) in N_2 flow atmosphere. The phenomenon is similar to that seen by Corr et al. [33].

Thus, in terms of the above electron microscopy studies, we consider that heating has a pronounced effect on the microstructure and morphology. As temperature increases, the microstructure and the morphology of the as-synthesized VO_2(B) drastically change from nano platelet-like VO_2(B) to submicron and micron subsphaeroidal VO_2(R/M), finally to a V_2O_3 sintered block.

2.4 Raman spectra analysis

All the Raman spectra of the as-prepared samples are shown in Fig.4, accompanying with the thermo spectral ID library index 451 (VO_2). In the wavelength range of 50~1200 cm^{-1}, all spectra are acquired with the same laser power and exposition time except V_2O_3. The absorption of V_2O_3 at the measure laser wavelength is high, making it necessary to apply more laser power to obtain identifiable Raman peaks [36].

The Raman spectrum of the as-synthesized VO_2(B) is presented as shown in curve a in Fig.4. It is dominated by the peaks at 104, 185, 257, 400, 464, 666 and 859 cm^{-1}. All these peaks are assigned to the Raman signature of VO_2(B) [37, 38]. The low-frequency peak at 104 cm^{-1} is corresponding to its rigid-layer modes. The peaks at 185 and 257 cm^{-1} are assigned to V-O-V bending modes and external modes (bending/wagging), respectively. The peaks at 400 and 464 cm^{-1} are attributed to V-O-V stretching modes. The peak at 666 cm^{-1} is due to coordination of vanadium atoms with three oxygen atoms, while the peak at 859 cm^{-1} is attributed to V=O stretching of distorted octahedra. These Raman results are in accordance with the above crystal structure analysis, and the results further confirm the formation of monoclinic VO_2(B).

Fig.4 curve d shows the Raman spectrum of sample S-750. There are 12 peaks at 140, 192, 221, 258, 307, 336, 387, 430, 495, 609, 662 and 816 cm^{-1}. All these peaks are the vibration bands of VO_2(M) and highly coincide with those reported in the previous works [39-43] and Thermo Spectral ID Library index 451 VO_2 (Fig.4 curve e). The results further confirm the formation of monoclinic VO_2(M). By the comparison of Fig.4 curve b and c, the Raman spectra of S-450 and S-600, we can find the coexistence of the monoclinic VO_2(B) and VO_2(M). The emergence of VO_2(M) is coupled with the decrease of the VO_2(B). These results are highly in agreement with those obtained in the XRD analysis.

Fig.4 curve f shows the Raman spectrum of sample S-1200. There are seven Raman peaks observed in our experiment. The major peaks at 213, 239, 295, 328, 501 and 589 cm^{-1} are coincided with literatures [36, 44]. These peaks are assigned to V_2O_3 E_g, A_{1g}, E_g, E_g, A_{1g}, and E_g phonon modes, respectively. The weak peaks located at 412 cm^{-1} can be assigned to the other E_g modes. Therefore, our results suggest all two A_{1g} and five E_g Raman active modes of V_2O_3 predicted by group theory [45]. The result also coincides with the above XRD analysis and further confirms the formation of V_2O_3.

In summary, all the Raman peaks depicted in Fig.4 are presented in Table 2, with the previous alongside the present findings on Raman shifts in VO_2(B), VO_2(M), and V_2O_3. As seen from Table 2, the present results agree very well with the previous findings. The Raman results also indicate that the obtained VO_2(B), VO_2(M), and V_2O_3 have good crystalline quality. They are consistent with the above XRD studies of similar samples as well and further confirm the crystal structure reconstruction during the thermal transition.

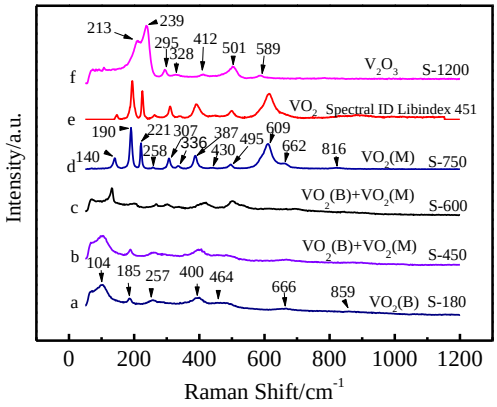

Fig.4 Raman spectra of annealed samples (a: S-180, b: S-450, c: S-600, d: S-750, e: Thermo Spectral ID Library index 451 VO_2, f: S-1200)

Table 2 Comparison of Raman data for VO_2(B), VO_2(M) and V_2O_3 in previous investigation with those of the present work (cm^{-1})

VO_2(B)			VO_2(M)			V_2O_3		
Present work	Ref. [37]	Ref. [38]	Present work	Ref. [39]	Ref. [40]	resent wor	Ref. [36]	Ref. [44]
104	103	118	-	-	-	-	-	-
-	-	-	140	142	149	-	-	-
185	195	191	192	191	199	213	203	210
-	-	-	221	223	225	239	231	234
-	-	-	258	262	259	-	-	-
257	295	270	-	-	265	-	-	-
-	-	-	307	310	313	295	290	290
-	-	-	336	-	339	328		327
400	391	399	387	392	392	412		-
-	-	-	-	-	395	-	-	-
-	-	-	430	443	444	-	-	-
-	-	-	-	-	453	-	-	-
464	-	-	-	-	489	-	-	-
-	-	-	495	500	503	501	500	501
-	-	-	609	613	595	589	590	595
-	-	-	-	-	618	-	-	-
666	662	670	662	-	670	-	-	-
859	-	880	816	-	830	-	-	-

3 Conclusions

1) Platelet-like monoclinic VO_2(B) can be synthesized via a facile hydrothermal process using a vanadium source of V_2O_5 and a reducing agent of oxalic acid.

2) The evolution of the crystal structure and morphology of monoclinic VO_2(B) to tetragonal VO_2(R), monoclinic VO_2(M) and corundum V_2O_3 can be tracked using XRD SEM and Raman spectroscopy.

3) VO_2(B) thermal transition can be obtained via the in situ XRD method, and it undergoes a reconstructive solid state phase transformation. Heating in N_2 flow atmosphere, the as-synthesized VO_2(B) is stable from room temperature to 420 ^{o}C, then transforms irreversibly into submicron and micron subsphaeroidal tetragonal VO_2(R) between 430 and 700 ^{o}C, and then the as-obtained VO_2(R) starts to decompose to form Magnéli phases V_nO_{2n-1} ($3 \le n \le 9$) series compounds at 1000 ^{o}C, and finally changes to a corundum structure V_2O_3 sintered block at ca. 1200 ℃.

References

1 Zhang Yifu, Zhang Juecheng, Zhang Xiongzhi *et al*. *Ceramics International*[J], 2013, 39: 8363

2 Tang Qing, Li Fengyu, Zhou Zhen *et al*. *Journal of Physical Chemistry C*[J], 2011, 115: 11 983

3 Whittaker L, Jaye C, Fu Zugen *et al*. *Journal of the American Chemical Society*[J], 2009, 131: 8884

4 Zhang Yifu, Zhang Juecheng, Zhang Xiongzhi *et al*. *Journal of Alloys and Compounds*[J], 2013, 570: 104

5 Huang Weigang, Lin Hua, Fan Qiaoqiao *et al*. *Rare Metal Materials and Engineering*[J], 2006, 35(10): 1554 (in Chinese)

6 Cao Chuanxiang, Gao Yanfeng, Luo Hongjie *et al*. *Journal of Physical Chemistry C*[J], 2008, 112: 18 810

7 McWhan D B, Marezio M, Remeika J P. *Physical Review B*[J], 1974, 10: 490

8 Andersson G. *Acta Chemica Scandinavica*[J], 1954, 8: 1599

9 Andersson G. *Acta Chemica Scandinavica*[J], 1956, 10: 623

10 Oka Y, Sato S, Yao T *et al*. *Journal of Solid State Chemistry*[J], 1998, 141: 594

11 Théobald F, Cabala R, Bernard J. *Journal of Solid State Chemistry*[J], 1976, 17: 431

12 Hagrman D, Zubieta J, Warren C J *et al*. *Journal of Solid State Chemistry*[J], 1998, 138: 178

13 Morin F J. *Physical Review Letters*[J], 1959, 3: 34

14 Zhang Shaohong, Fu Juan, Su Qiucheng *et al*. *Rare Metal Materials and Engineering*[J], 2015, 44(3): 738 (in Chinese)

15 Yan Jiazhen, Zhang Yue, Liu Yangsi *et al*. *Rare Metal Materials and Engineering*[J], 2008, 37(9): 1649 (in Chinese)

16 Zhao Lili, Miao Lei, Tanemura S *et al*. *Thin Solid Films*[J], 2013, 5: 157

17 Yin Haihong, Ni Juan, Jiang Wentao *et al*. *Physica E*[J], 2011, 43: 1720

18 Greenberg C B. *Thin Solid Films*[J], 1994, 251: 81

19 Chen Sihai, Ma Hong, Yi Xinjian *et al*. *Infrared Physics & Technology*[J], 2004, 45: 239

20 Kim H T, Chae B G, Youn D H *et al*. *New Journal of Physics*[J], 2004, 6: 52

21 Ni Juan, Jiang Wentao, Yu Ke *et al*. *Electrochimica Acta*[J], 2011, 56: 2122

22 Li Wu, Dahn J R, Wainwright D S. *Science*[J], 1994, 264: 1115

23 Tsang C, Manthiram A. *Journal of the Electrochemical Society*[J], 1997, 144: 520

24 Baudrin E, Sudant G, Larcher D *et al*. *Chemistry of Materials*[J], 2006, 18: 4369

25 Zhang Yifu, Fan Meijuan, Zhou Min *et al*. *Bulletin of Materials Science*[J], 2012, 35: 369

26 Liu Xinghai, Huang Chi, Yi Shengping *et al*. *Solid State Communications*[J], 2007, 144: 259

27 Leroux C, Nihoul G, Van Tendeloo G. *Physical Review B*[J], 1998, 57: 5111

28 Murphy D W, Christian P A, DiSalvo F J *et al*. *Journal of the Electrochemical Society*[J], 1981, 128: 2053

29 Valmalette J C, Gavarri J R. *Materials Science & Engineering B*[J], 1998, 54: 168

30 Li Zhiyou, Cao Dumeng, Zhou Kechao. *Transactions of Nonferrous Metals Society of China*[J], 2007,17: 720

31 Li Zhiyou, Cao Dumeng, Zhou Kechao. *Rare Metal Materials and Engineering*[J], 2006, 35 (S2): 316 (in Chinese)

32 Blanton T N, Zdzieszynski S, Nicholas M *et al*. *Advances in X-Ray Analysis*[J] 2005, 48: 27

33 Corr S A, Grossman M, Shi Yifeng *et al*. *Journal of Materials Chemistry*[J], 2009, 19: 4362

34 Schwingenschlgöl U, Eyert V. *Annalen der Physik*[J], 2004, 13: 475

35 Liu Junfeng, Li Qiuhong, Wang Taihong *et al*. *Angewandte Chemie International Edition*[J], 2004, 116: 5158

36 Kuroda N, Fan H Y. *Physical Review B*[J], 1977, 16: 5003

37 Wang Xuejin, Fei Yunjie, Xiong Yanyun *et al*. *Chinese Journal of Light Scattering*[J], 2002, 13: 235

38 Huang Chunming, Chen Lihua, Xu Gang *et al*. *Journal of Sol-Gel Science and Technology*[J], 2012, 63: 103

39 Parker J C. *Physical Review B* [J], 1990, 42: 3164

40 Schilbe P. *Physica B*[J], 2002, 316-317: 600

41 Hu Wenliang, Xu Gang, Ma Jianwei *et al*. *Acta Physico-Chimica Sinica*[J], 2012, 28(6): 1533

42 Julien C, Nazri G A, Bergström O. *Physica Status Solidi B*[J], 1997, 201: 319

43 Wang Xuejin, Liang Chunjun, Guan Kangping *et al*. *Chinese Physics B*[J], 2008, 17(9): 3512

44 Tatsuyama C, Fan H Y. *Physical Review B*[J], 1980, 21(7): 2977

45 Misochko O V, Tani M, Sakai K *et al*. *Physical Review B*[J], 1998, 58 (19): 12 789

VO_2(B)热转化为 VO_2(R)和 V_2O_3 的高温 XRD 原位表征

张少鸿，付 娟，苏秋成，吴梁鹏，李新军

(中国科学院广州能源研究所，广东 广州 510640)

摘 要：以草酸和V_2O_5为原料，采用水热法制备VO_2(B)。通过高温原位X射线衍射技术研究VO_2(B)在氮气保护下升高温度过程中的相变特性，采用X射线衍射仪 (XRD)、场发射扫描电子显微镜(FE-SEM)和激光拉曼光谱技术分析所制备样品及其在不同温度热相变产物的微观形貌、晶体结构和物相组成。结果表明：以草酸和V_2O_5为原料，用水热法可制得单斜晶系VO_2(B)，颗粒呈纳米片状；升温至430~700 ℃之间，VO_2(B)不可逆转化为四方晶系VO_2(R)，形貌由纳米片状变为亚微米及微米近球形；升温至1000 ℃左右，VO_2(R)开始分解形成Magnéli 相系列化合物（V_nO_{2n-1}，$3 \leqslant n \leqslant 9$）；升温至约1200 ℃完全转变为具有刚玉结构的 V_2O_3 烧结块。

关键词：水热法；氧化钒；原位 XRD；热相变；拉曼光谱

作者简介：张少鸿，男，1965 年生，高级工程师，中国科学院广州能源研究所，中国科学院可再生能源重点实验室，广东 广州 510640，电话：020-37246206，E-mail: zhangsh@ms.giec.ac.cn